THE ASTROPHYSICAL JOURNAL, 378:227–238, 1991 September 1

THE CONTRIBUTION OF LIGHT BENDING AND REDSHIFT TO THE PULSE CHARACTERISTICS OF A PULSAR IN THE CASE OF SMALLER NEUTRON STARS

R. C. KAPOOR
Indian Institute of Astrophysics, Koramangala, Bangalore 560034, India
Received 1990 August 27; accepted 1991 February 26

ABSTRACT

An estimate has been made of the effect of light bending and redshift on the pulsar beam characteristics using the weak form of the Kerr metric, applicable to a slow-rotating neutron star. The calculations refer to the canonical narrow conical beam model of pulsar emission from a 1.4 $M_\odot$ neutron star with radii in the range $R = 6$–10 km and periods of 33 and 1.56 ms. The beam is found to diverge by a factor of 2 or less and to suffer an intensity reduction by an order of magnitude when emitted from close to the star's surface. This flattening of the pulse profile apparently is strongest for the smallest of the neutron stars, becoming insignificant for emission points located beyond $\simeq 20$ km for all the neutron star radii considered. For a given emission location, the divergence is comparatively greater in the Schwarzschild background than in the rotational case, since, by virtue of the rotational terms in the metric, an aberration effect comes into play, which always tends to reverse the flattening effect of spacetime curvature by slightly squeezing the pulse in longitude. For instance, for a pulse emitted in the equatorial plane from beyond ~ 30 km in the case of the 1.56 ms period, aberration is so strong that it overcomes the divergence effect. This will result in an apparent reduction of the duty cycle. Although the pulse must brighten up, a large redshift factor overcomes this to keep the pulse profile flattened. For the larger of the periods, the squeezing is noticeably present at emission points ~ 500 km from the star's surface. For the same radial location, the squeezing is found to be less severe for emission at lesser inclination angles.

Subject headings: pulsars — relativity — stars: neutron

1. INTRODUCTION

The general relativistic effects of spacetime curvature and rotation on the radiation characteristics of pulsars have been the subject of investigation in the recent past. Applying the basic formalism developed in Kapoor (1979, 1981) to the case of slow rotation, Kapoor & Datta (1985, 1986) indicated modifications in the beamwidth and arrival times of pulses from a millisecond pulsar as introduced by the general relativistic effects of light bending and the dragging of inertial frames. Mészáros & Riffert (1987, 1988) have investigated the modifications introduced by spacetime curvature on the beaming, spectra, and pulse properties of accreting neutron stars and pulsars. However, according to them, best-fit models consistent with the observational evidence of X-ray pulsars and QPOs may be obtained by taking smaller radii than the conventional figure of 10 km—namely, a neutron star radius R as small as 1.5 R_S for a mass of $M = 1.4\ M_\odot$ ($R_S = 4.1$ km) is suggested. An estimate of the effective temperature from X-ray burst characteristics leads to radii in the range $R = 6$–12 km, assuming luminosity to be at the appropriate Eddington values (Joss & Rappaport 1984; London, Taam, & Howard 1985). Similarly, the interpretations of observations of X-ray burst sources by some other groups (see Mészáros & Riffert 1987 for references) also indicate the possibility of neutron star radii in the range 1.6–2 R_S. One therefore asks, given that the radii were smaller than the conventional figure of $R = 10$ km, how strong are the effects of general relativity on the beaming and the other characteristics of the pulsed radiation from pulsars (J. Rankin 1990, private communication).

The purpose of this paper is to investigate these effects using the weak form of the Kerr metric appropriate for a small specific angular momentum parameter for $M = 1.4\ M_\odot$ and the neutron star radii in the range $R = 6$–10 km. Smaller neutron star radii will be allowed only by the softest equations of state. However, our intention here is *not* to address the issue of smaller neutron stars from the point of view of equation-of-state considerations or to interpret observational data to make a case for the existence of such small stars. Rather we consider their case mainly for a study of photon propagation in their background in the geometrical optics approximation. An $R = 6$ km, 1.4 $M_\odot$ nonrotating neutron star is within the upper bound of 0.854 for its gravitational redshift as deduced by Lindblom (1984) and will be of academic interest, since its surface lies inside its photon spheres. Since we confine our attention here to the popular model of pulsar emission proposed by Radhakrishnan & Cooke (1969), where the width of the conical pulsar beam is $\sim 10°$, photon trapping by the neutron star will not be of concern here. The calculations have been performed for two values of the period of rotation, namely, $P = 33$ ms and $P = 1.56$ ms. Preliminary results are given in Kapoor (1990), and here we assess in detail the contribution of frame drag and Doppler effect to the bending in the photon trajectories leading to longitudinal asymmetries of the pulsed radiation, and arrival time differences of pulses starting from different altitudes.

The format of the paper is as follows. Section 2 briefly reviews photon propagation in a weak Kerr geometry, whereas in § 3 the calculation of the consequent change in the pulse profile is given. Section 4 deals with the effects of spacetime curvature and rotation on the relative arrival time of pulses. Results on the pulse characteristics and their implications in view of a similar recent investigation by Bhatia et al. (1988) are discussed in § 5.

2. PHOTON TRAJECTORIES IN THE WEAK KERR GEOMETRY

The metric we adopt to describe the spacetime geometry around a rotating neutron star has the signature + − − − and $G = c = 1$:

$$ds^2 = e^{2\nu}dt^2 - e^{2\psi}(d\varphi - \omega\, dt)^2 - e^{2\mu}d\theta^2 - e^{2\lambda}dr^2 , \quad (1)$$

where for the case of the Kerr metric (Chandrasekhar 1983)

$$e^{2\nu} = \frac{\rho^2\Delta}{\Sigma^2} , \quad e^{2\psi} = \frac{\Sigma^2 \sin^2\theta}{\rho^2} , \quad e^{2\lambda} = \frac{\rho^2}{\Delta} , \quad e^{2\mu} = \rho^2 ,$$

$$\rho^2 = r^2 + a^2\cos^2\theta , \quad \Delta = r^2\left(1 - \frac{2m}{r}\right) + a^2 , \quad (2a)$$

$$\Sigma^2 = (r^2 + a^2) - a^2\Delta \sin^2\theta .$$

The quantity

$$\omega = \frac{2amr}{\Sigma^2} = \frac{2Jr}{\Sigma^2} \quad (2b)$$

is the angular velocity of dragging of inertial frames, a is the specific angular momentum of the rotating mass ($= J/m$), and J is the total angular momentum. Since for both the periods of rotation of interest here, $a \lesssim 0.2m$, terms in the Kerr metric with a^2/r^2 will be neglected. Such an approximation, we believe, will not jeopardize the qualitative nature of the results. The basic formalism we have used to determine photon trajectories is mainly the same as that in Kapoor (1979, 1981) extended to the case of slow rotation in Kapoor & Datta (1984, 1985, 1986) and is summarized below. We assume that the source of radiation at $r_{\rm em}$, θ_e is monochromatic, following a corotational circular orbit. Its four-velocity vector is $u^\alpha = dx^\alpha/ds$, with

$$u^0 = \frac{dt}{ds} = e^{-\nu}(1 - V_e^2)^{-1/2} , \quad \frac{dr}{ds} = 0 , \quad V_e = e^{\psi-\nu}(\Omega - \omega) . \quad (3)$$

Here Ω is the angular velocity of the emitter $= (d\phi/ds)/(dt/ds)$ as measured by a remote observer at $r = r_0 (\gg 2m)$ who is necessarily a relativist. The quantity V_e in equation (3) above is the emitter's tangential velocity as seen by a locally nonrotating observer who revolves around the star with an angular velocity ω. The observed pulsar radiation is assumed to be emitted in a cone pattern centered along the magnetic axis. The trajectory of a photon emitted in a general direction will be bent because of spacetime curvature and dragged away because of the rotational effects from the original direction of its emission. For our purpose, it is sufficient to consider the simple case of central line-of-sight photons in the conical beam whose axis is inclined at an angle θ_e with respect to the axis of rotation. Since pulsars are general relativistically slow rotators, the polar bending in the photon trajectories will be small compared with the azimuthal bending, so that photons emitted at θ_e can be regarded as continuing to be moving with $\theta_e \cong$ constant, which then is the inclination angle of the star as seen by the remote observer. In this approximation, the bending amounts to

$$-\varphi_0 = \int_{r_{\rm em}}^{r_0} \frac{d\phi/d\Gamma}{dr/d\Gamma}\, dr = \int_{r_{\rm em}}^{r_0} f(r, q_{\rm em})\, dr , \quad (4)$$

where Γ is an affine parameter. The function $f(r, q_{\rm em})$ is evaluated by solving the geodesic equations of motion of the photon in the geometrical optics approximation and has the form (Kapoor & Datta 1985)

$$f = \frac{\omega(1 + \omega q_{\rm em}) - q_{\rm em}\, e^{2\nu - 2\psi}}{e^{\nu-\lambda}[(1 + \omega q_{\rm em})^2 - q_{\rm em}^2\, e^{2\nu-2\psi}]^{1/2}} , \quad (5)$$

where the quantity $q_{\rm em}$ is the impact parameter of the photon. It can be first evaluated at the point of emission in the frame of reference of the locally nonrotating observer for a photon emitted at an angle δ' with respect to the radial direction in his reference frame. Then a Lorentz transformation to the local rest frame of the star through

$$\sin\delta = \frac{\sin\delta' - V_e}{1 - V_e \sin\delta'} \quad (6)$$

gives

$$q_{\rm em} = \frac{(V_e + \sin\delta)e^{\psi-\nu}}{1 + e^{\psi-\nu}(\omega V_e + \Omega \sin\delta)} \quad (7)$$

for a photon emitted at an azimuthal angle δ with respect to the radius vector in the local rest frame of the emitter. The angle δ increases in a direction opposite to that of rotation of the star, such that $\delta = -\pi/2$ for a tangential forward photon and $\delta = 0$ for a radial outward photon, and so on.

The presence of rotational terms in the formalism outlined above implies that the entire beam will be tilted in the direction of rotation of the star. This tilt, which is to be understood in terms of the net bending of a $\delta = 0$ (radial outward) photon, is given approximately by equation (4) as

$$-\varphi_0(\delta = 0) \approx \int \frac{\omega\, dr}{e^{2\nu}} - q_{\rm em}\int \frac{dr}{e^{2\psi}} = \Theta - \frac{q_{\rm em}(\delta = 0)}{\sin^2\theta_e\, r_{\rm em}} , \quad (8)$$

where

$$\Theta = -\frac{a}{m}\left[\frac{m}{r_{\rm em}} + \frac{1}{2}\ln\left(1 - \frac{2m}{r_{\rm em}}\right)\right] . \quad (9)$$

In equation (8) we have assumed $\omega q_{\rm em} \ll 1$, which is justified by our calculations of the bending of trajectories from equation (4). The quantity

$$\Theta = \int \frac{\omega\, dt}{dr} = \int \frac{\omega\, dr}{e^{2\nu}} \quad (10)$$

appearing in equations (8) and (9) above is in its own right the angle by which the plane of polarization will be rotated as a result of the dragging of inertial frames when the photon is emitted along the axis of rotation. Equation (10) (valid for $\theta_e = 0$) gives $\Theta \simeq 1°$ for emission from near the surface; for $\theta_e = \pi/2$, Θ will be zero. In the absence of a reference, however, this quantity is of academic interest only.

The time of emission of the photon $t = t_e$ and that of reception at the remote observer $t = T$ are related through

$$T - t_e = \int_{r_{\rm em}}^{r_0} g(r, q_{\rm em})\, dr , \quad (11)$$

with

$$g = \frac{1 + \omega q_{\rm em}}{e^{2\nu}[(1 + \omega q_{\rm em})^2 - q_{\rm em}^2\, e^{2\nu-2\psi}]^{1/2}} . \quad (12)$$

3. THE PULSE PROFILE

A conical beam of radiation ($-\delta_e \leq \delta \leq \delta_e$) emitted in a direction away from the surface of the neutron star will diverge as a result of bending in the trajectories of photons climbing the potential well. In a Schwarzschild spacetime, $|\varphi_0|$ is symmetrical with respect to $\pm\delta$ and so will be the profile in longitude. However, the function of rotational terms is to introduce a bit of an extra bending in the direction of rotation of the star such that the pulse profile will be longitudinally asymmetrical when received at r_0. Referring to Figure 1, a photon emitted from the emission point $r = r_{em} \geq R$, at an angle δ with respect to the radius vector, emerges at an angle δ_0 at r_0. This angle can be found by evaluating the bending of the photon as given by equation (4):

$$-\varphi_0(\delta) = \delta_0 \,. \tag{13}$$

The beam diverges when $\delta_0 > \delta$. This widening can be described by a quantity called the divergence index:

$$\Delta = \Delta(\delta, r_{em}) = \frac{d\delta_0}{d\delta} = -\frac{d\varphi_0}{d\delta}\bigg|_{r_{em}} . \tag{14}$$

Because of rotation, $\Delta(+\delta) \neq \Delta(-\delta)$. This in essence implies a longitudinal asymmetry of the pulse that can be characterized by $\Delta^+ - \Delta^-$. This difference will be zero when $\delta = 0$. Associated with the divergence is reduction in the intensity in the beam, which can be understood in terms of conservation of the energy flux. This is measured by a factor

$$\epsilon(\delta) = \frac{\sin\delta\, d\delta}{\sin\delta_0\, d\delta_0} = \frac{1}{\Delta}\frac{\sin\delta}{\sin\delta_0} . \tag{15}$$

There will be deamplification, i.e., $\epsilon < 1$, when $\delta_0 > \delta$. For the case of emission close to the axis of the conical beam,

$$\epsilon(\delta \simeq 0)|_{rot} \simeq \frac{1}{\Delta}\frac{\delta}{\delta_0} \simeq \frac{1}{\Delta^2} . \tag{16a}$$

In the Schwarzschild case, $\Delta(\delta \to 0) \to (1 - 2m/r_{em})^{-1/2}$, so that

$$\epsilon(\delta \simeq 0)|_{Schw} \simeq \left(1 - \frac{2m}{r_{em}}\right) . \tag{16b}$$

In accordance with the Liouville's theorem, there is a reduction in the intensity due to redshift as well. We calculate the net deamplification ϵ_n in the beam from the new intensity $I_n(\delta_0)$ as

$$\epsilon_n = \frac{I_n(\delta_0)}{I_e(\delta)} = \frac{\epsilon}{[1 + z(\delta)]^3} . \tag{17}$$

The quantity $I_e(\delta)$ is the intensity at the emission frequency ν_e in the rest frame of the emitter and is assumed to have a steep Gaussian form. An explicit expression for redshift (see, e.g., Kapoor 1981; Kapoor & Datta 1984) is

$$\frac{\nu_e}{\nu} = 1 + z(\delta) = \frac{1 + \Omega q_{em}}{e^{\nu}(1 - V_e^2)^{1/2}} . \tag{18}$$

Equations (17)–(18) imply that because of slight Doppler boosting and diminution, respectively, $I_n(-\delta_0)$ will slightly exceed $I_n(+\delta_0)$. It may be noted that the index Δ in equation (14) differs from that in Kapoor & Datta (1985), where addition of the angle δ to φ_0 to give δ_0 is redundant and leads to an overestimate of divergence in the conical beam. While this does affect some of the results by lessening the beam divergence and the attendant deamplification by a factor ~ 2 (see Bhatia et al. 1988), the main conclusions remain largely unaffected or require a minor qualification. To make the results more transparent, we have evaluated the net deamplification ϵ_n without normalizing the deamplification factor ϵ as earlier. As will be made clear, equation (17) here is more appropriate for our discussion of general relativistic effects of curvature and rotation on the beam characteristics.

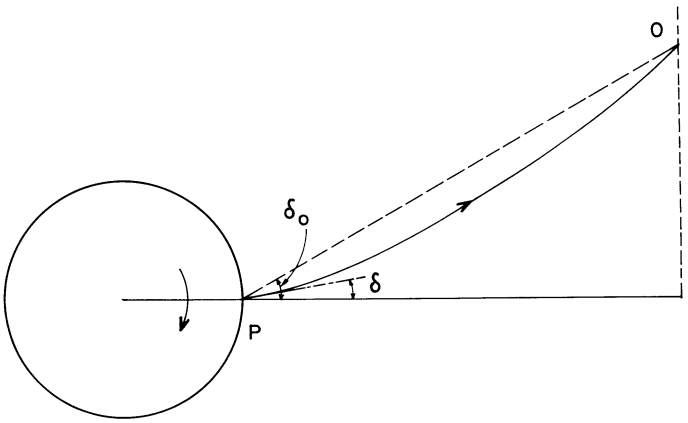

FIG. 1.—Schematic illustration of the photon trajectory in terms of the angle of emission δ and δ_0.

4. THE ADVANCEMENT IN ARRIVAL TIME OF PULSES

In the canonical magnetic polar cap models, the frequency of the emitted coherent radiation is a function of the radial location of the emitter (the radius-to-frequency mapping) such that a relatively higher frequency pulse emanates from a region closer to the surface of the neutron star. For two simultaneously emitted beams from r_{em} and $r_{em} + \Delta r$, the arrival times will differ by the light travel time $\Delta\tau_{ret}$ over the distance Δr, corrected for retardation. It follows from the geodesic equations of motion for the photons that

$$\Delta\tau_{ret} = \int_{r_{em}}^{r_{em}+\Delta r} g(r, q_{em})\, dr \,. \tag{19}$$

Now the dragging of inertial frames essentially makes a radially outgoing photon ($\delta = 0$) suffer a net deflection, $\varphi_0(\delta = 0)$ in the direction of rotation of the star, whose magnitude increases as the emission point is shifted outward. Consequently, for the two simultaneously emitted pulses from r_{em} and $r_{em} + \Delta r$, a phase shift will be introduced to further advance the arrival time of the pulse from $r_{em} + \Delta r$ over that from r_{em} (Kapoor & Datta 1986) by an amount

$$\Delta r_{drag} = \frac{P}{2\pi}\,[\,|\varphi_0(r_{em} + \Delta r, \theta_e, \delta = 0)| - |\varphi_0(r_{em}, \theta_e, \delta = 0)|\,] , \tag{20}$$

where P is the period of the pulsar. The net arrival time advancement of the lower frequency pulse over that of the higher frequency pulse is

$$\Delta\tau = \Delta\pi_{ret} + \Delta\tau_{drag} \,. \tag{21}$$

Here it may be pointed out that the evaluation of the arrival time advancement refers to the peaks of the pulses of the mid-

point of an average pulse profile with a more detailed structure. This is to be distinguished from the arrival time differences for photons within the same conical beam, to be mentioned later.

5. RESULTS AND DISCUSSION

In order to determine the effect of spacetime curvature and rotation on the beaming and the pulse characteristics of a pulsar with a radius smaller than the conventional figure of 10 km, we take $M = 1.4\ M_\odot$ which is a representative choice consistent with the available binary pulsar data. The simplest form of the beam considered here is a conical one, which at the point of emission has an angular width $W_e = 2\delta_e$ with $\delta_e = \pm 5°$ and a steep Gaussian distribution in intensity. The theoretical framework, though, is general and will apply to any emission model and initial pulse profile. The calculations have been performed for two well-known pulsar periods, namely, 1.56 and 33 ms. The various neutron star parameters are listed in Table 1, where $J = \frac{2}{5}MR^2\Omega$. It may be noted that an $R = 6$ km star with 33 ms period has its surface inside both its retrograde and prograde photon spheres, whereas the one with the 1.56 ms period has its surface inside the retrograde photon sphere r_{ph}. For the former case, tangential forward and backward photons, and for the latter case tangential backward photons emitted from $r_{em} \leq r_{ph}$, will be trapped in the star. However, this should not cause concern here, since we consider only a radially outward-directed narrow beam of radiation for which the amount of net bending is too small, despite a large spacetime curvature, to lead to any pruning of the beam in longitude.

The bending of photon trajectories and the resultant pulse profile have been calculated for various values of the polar angle of emission, for $r_{em} = R$, $2R$, $3R$, and $5R$ in the weak Kerr as well as the Schwarzschild background. The results are presented in Tables 2–5. The main feature that these calculations bring out is that the conical beam emanating from near the surface diverges by a factor of 2 or less, and the intensity is reduced by an order of magnitude or less. We notice that the larger the neutron star, the less the divergence and the less the intensity reduction of the beam caused by spacetime curvature. However, the effect is mainly distance-dependent and dwindles fast as r_{em} is shifted outward, becoming insignificant once $r_{em} \simeq 20$ km, regardless of the neutron star radius. Figure 2 shows the resultant pulse profiles for some of the neutron star radii (6, 8, and 10 km) and for different values of θ_e and r_{em}. It may be pointed out that the profiles for $R = 6$ km and $r_{em} = 5R$ are very similar to those for $R = 10$ km and $r_{em} = 3R$. The amount of bending of the photon trajectories is nearly linear in δ for small values of δ. The slight longitudinal asymmetry introduced in the pulse profile by the dragging of inertial frames [hence $\Delta(+\delta, r_{em}) \neq \Delta(-\delta, r_{em})$] can be noticed more explicitly in the magnitude of $\varphi_0(\pm\delta)$ with respect to the pulse center ($\delta = 0$) than in Figure 2. The longitudinal asymmetry is also not uniform but decreases slowly with δ, i.e., as one goes from the ascending end ($\delta_e = -5°$) of the pulse to the descending end ($\delta_e = +5°$). The ascending part of the profile is stretched and Doppler-boosted, whereas the descending part is compressed and Doppler-diminished. This is indicated by the gradual decrease in the ϵ_n values as the angle δ is increased from $-\delta_e$ through $\delta = 0$ to $+\delta_e$. This holds for all the neutron star radii and r_{em} considered. The divergence effect will be nil for the light-cylinder model, where a tangential relativistic beam ($\delta = \pm\pi/2$) has $\Delta \simeq 0$.

Referring to Tables 2–5, we notice that the values of $\varphi_0(\delta)$ in the Schwarzschild geometry slightly exceed those in the Kerr geometry. The difference is small but not unimportant. It arises from a squeezing effect on the beam resulting from aberration in the rotational case, which always acts to reduce the divergence due to the spacetime curvature. To elaborate on this, let us take the case of an $R = 10$ km neutron star with $P = 1.56$ ms, $\theta_e = \pi/2$, and $r_{em} = R$. In the Schwarzschild background, the $-5°$ photon emerges at 6°.533 longitude. Because of symmetry, the width of the pulse is twice this, so that a beamwidth $W_e = 10°$ in the emitter's frame is increased to $W_{0(\mathrm{Schw})} = 13°.066$ (the sum of the bending angles of $\pm\delta_e$ photons) as determined by the remote observer. When one includes the effects of rotation, symmetry will no longer be there. The $\delta_e = -5°$ photon this time is mapped at 6°.447 whereas the $+5°$ one is mapped at $-6°.333$ longitude. This gives $W_{0(\mathrm{Kerr})} = 12°.78$, a figure slightly less than its Schwarzschild counterpart. This is because of aberration, which reduces Δ by squeezing the pulse—more so if r_{em} is large. In such a case, the squeezing effect on the beam becomes so large that it can overcome any divergence caused by the spacetime curvature. In other words, there is a reversal in the value of Δ from $\Delta > 1$ to $\Delta < 1$. This can be inferred from the fact that at $r_{em} \gg R$, the observed

TABLE 1

NEUTRON STAR PARAMETERS

R (km)	J (10^{48} cgs)	a/m	r_{ph} Retrograde (km)	r_{ph} Prograde (km)	r_{ph} Schwarzschild (km)	$\omega(R)/\Omega$
			$M = 1.4\ M_\odot$; $P = 1.56$ ms			
6.....	1.616	0.094	6.422	5.974	6.202	0.276
7.....	2.200	0.128	6.499	5.889	6.202	0.236
8.....	2.874	0.167	6.588	5.790	6.202	0.207
9.....	3.673	0.210	6.687	5.676	6.202	0.184
10.....	4.490	0.260	6.796	5.545	6.202	0.165
			$M = 1.4\ M_\odot$; $P = 33$ ms			
6.....	0.076	0.004	6.212	6.191	6.202	0.276
7.....	0.104	0.006	6.216	6.187	6.202	0.236
8.....	0.136	0.008	6.221	6.183	6.202	0.207
9.....	0.172	0.010	6.226	6.178	6.202	0.184
10.....	0.212	0.012	6.231	6.172	6.202	0.165

TABLE 2

$r_{em} = R$

R (km)	V_e/c	$\varphi_0(+5°)$	Z^+	Δ^+	I_n^+/I_e	$\varphi_0(-5°)$	Z^-	Δ^-	I_n^-/I_e
				$P = 1.56$ ms; $\theta_e = 0.3\pi$ (Weak Kerr)					
6.....	0.085	−10.928	6.171	2.176	0.034	11.051	5.812	2.226	0.035
7.....	0.091	−9.510	4.107	1.892	0.068	9.624	3.865	1.938	0.070
8.....	0.099	−8.738	3.231	1.738	0.102	8.849	3.032	1.782	0.105
9.....	0.109	−8.245	2.761	1.639	0.134	8.357	2.580	1.684	0.138
10.....	0.119	−7.899	2.474	1.569	0.164	8.013	2.302	1.615	0.168
				$P = 1.56$ ms; $\theta_e = \pi/2$ (Weak Kerr)					
6.....	0.105	−8.785	6.343	1.747	0.051	8.909	5.896	1.797	0.053
7.....	0.112	−7.643	4.231	1.519	0.102	7.757	3.929	1.564	0.105
8.....	0.123	−7.018	3.343	1.394	0.153	7.129	3.093	1.438	0.156
9.....	0.134	−6.617	2.870	1.313	0.201	6.728	2.644	1.358	0.207
10.....	0.147	−6.334	2.586	1.256	0.243	6.447	2.371	1.301	0.252
				$P = 1.56$ ms; $\theta_e = \pi/2$ (Schwarzschild)					
6.....	...	−9.010	6.176	1.805	0.050	...	5.724	1.805	0.054
7.....	...	−7.837	4.097	1.569	0.099	...	3.767	1.569	0.108
8.....	...	−7.206	3.213	1.442	0.150	...	2.962	1.442	0.163
9.....	...	−6.808	2.735	1.362	0.197	...	2.509	1.362	0.215
10.....	...	−6.533	2.441	1.307	0.240	...	2.227	1.307	0.263
				$P = 33$ ms; $\theta_s = \pi/2$ (Weak Kerr)					
6.....	0.005	−8.974	5.772	1.797	0.054	8.979	5.752	1.779	0.054
7.....	0.005	−7.815	3.823	1.563	0.107	7.820	3.809	1.566	0.107
8.....	0.006	−7.190	2.982	1.439	0.162	7.195	2.970	1.441	0.163
9.....	0.006	−6.796	2.520	1.359	0.215	6.801	2.510	1.361	0.215
10.....	0.007	−6.523	2.231	1.305	0.264	6.528	2.221	1.307	0.264

NOTE.—$Z^{\pm} = [1 + z(\pm 5°)]^3$; $\varphi_0(\delta = 0)$ has been subtracted from $\varphi_0(\pm 5°)$ values.

TABLE 3

$r_{em} = 2R$

R (km)	V_e/c	$\varphi_0(+5°)$	Z^+	Δ^+	I_n^+/I_e	$\varphi_0(-5°)$	Z^-	Δ^-	I_n^-/I_e
				$P = 1.56$ ms; $\theta_e = 0.3\pi$ (Weak Kerr)					
6.....	0.156	−7.480	2.190	1.487	0.206	7.579	2.021	1.526	0.214
7.....	0.176	−7.180	2.034	1.426	0.241	7.289	1.860	1.469	0.251
8.....	0.197	−6.961	1.959	1.381	0.266	7.081	1.776	1.429	0.279
9.....	0.218	−6.791	1.931	1.346	0.284	6.920	1.737	1.398	0.298
10.....	0.239	−6.649	1.937	1.316	0.925	6.789	1.729	1.372	0.311
				$P = 1.56$ ms; $\theta_e = \pi/2$ (Weak Kerr)					
6.....	0.193	−6.000	2.339	1.191	0.299	6.098	2.124	1.230	0.314
7.....	0.218	−5.746	2.208	1.139	0.346	5.854	1.985	1.182	0.364
8.....	0.244	−5.557	2.166	1.100	0.378	5.675	1.929	1.147	0.398
9.....	0.270	−5.405	2.180	1.069	0.397	5.532	1.925	1.120	0.419
10.....	0.296	−5.275	2.236	1.042	0.407	5.412	1.959	1.097	0.430
				$P = 1.56$ ms; $\theta_e = \pi/2$ (Schwarzschild)					
6.....	...	−6.177	2.108	1.236	0.311	...	1.899	1.236	0.345
7.....	...	−5.955	1.936	1.194	0.364	...	1.721	1.194	0.409
8.....	...	−5.803	1.840	1.161	0.404	...	1.614	1.161	0.460
9.....	...	−5.692	1.789	1.139	0.431	...	1.548	1.139	0.498
10.....	...	−5.608	1.766	1.122	0.450	...	1.508	1.122	0.527
				$P = 33$ ms; $\theta_e = \pi/2$ (Weak Kerr)					
6.....	0.010	−6.169	1.889	1.234	0.348	6.174	1.880	1.236	0.349
7.....	0.010	−5.948	1.696	1.189	0.417	5.953	1.686	1.191	0.418
8.....	0.011	−5.797	1.571	1.159	0.474	5.802	1.562	1.161	0.475
9.....	0.013	−5.686	1.485	1.137	0.521	5.693	1.475	1.139	0.523
10.....	0.014	−5.602	1.422	1.120	0.561	5.609	1.411	1.123	0.563

NOTE.—$Z^{\pm} = [1 + z(\pm 5°)]^3$; $\varphi_0(\delta = 0)$ has been subtracted from $\varphi_0(5°)$ values.

TABLE 4

$r_{em} = 3R$

R (km)	V_e/c	$\varphi_0(+5°)$	Z^+	Δ^+	I_n^+/I_e	$\varphi_0(-5°)$	Z^-	Δ^-	I_n^-/I_e
$P = 1.56$ ms; $\theta_e = 0.3\pi$ (Weak Kerr)									
6.....	0.221	−6.800	1.939	1.348	0.282	6.926	1.744	1.398	0.296
7.....	0.253	−6.596	1.958	1.306	0.297	6.737	1.741	1.362	0.314
8.....	0.289	−6.426	2.029	1.270	0.302	6.583	1.786	1.333	0.319
9.....	0.317	−6.276	2.145	1.239	0.300	6.447	1.871	1.307	0.317
10.....	0.349	−6.135	2.303	1.209	0.293	6.321	1.994	1.284	0.309
$P = 1.56$ ms; $\theta_e = \pi/2$ (Weak Kerr)									
6.....	0.273	−5.416	2.193	1.071	0.393	5.541	1.937	1.121	0.416
7.....	0.312	−5.227	2.292	1.032	0.404	5.367	2.002	1.088	0.428
8.....	0.352	−5.063	2.470	0.998	0.401	5.217	2.138	1.059	0.423
9.....	0.392	−4.911	2.726	0.966	0.387	5.077	2.343	1.033	0.497
10.....	0.432	−4.762	3.070	0.935	0.366	4.911	2.628	1.007	0.382
$P = 1.56$ ms; $\theta_e = \pi/2$ (Schwarzschild)									
6.....	...	−5.693	1.789	1.139	0.431	...	1.548	1.139	0.498
7.....	...	−5.573	1.763	1.115	0.457	...	1.495	1.115	0.538
8.....	...	−5.488	1.780	1.098	0.466	...	1.479	1.098	0.561
9.....	...	−5.426	1.831	1.085	0.464	...	1.489	1.085	0.571
10.....	...	−5.375	1.912	1.075	0.453	...	1.523	1.075	0.568
$P = 33$ ms; $\theta_e = \pi/2$ (Weak Kerr)									
6.....	0.013	−5.686	1.485	1.137	0.521	5.692	1.475	1.139	0.523
7.....	0.015	−5.567	1.396	1.113	0.578	5.574	1.385	1.112	0.581
8.....	0.017	−5.482	1.335	1.096	0.624	5.490	1.324	1.099	0.626
9.....	0.019	−5.418	1.291	1.083	0.660	5.426	1.279	1.086	0.664
10.....	0.020	−5.368	1.258	1.073	0.690	5.377	1.245	1.076	0.694

NOTE.—$Z^{\pm} = [1 + z(\pm 5°)]^3$; $\varphi_0(\delta = 0)$ has been subtracted from $\varphi_0(\pm 5°)$ values.

TABLE 5

$r_{em} = 5R$

R (km)	V_e/c	$\varphi_0(+5°)$	Z^+	Δ^+	I_n^+/I_e	$\varphi_0(-5°)$	Z^-	Δ^-	I_n^-/I_e
$P = 1.56$ ms; $\theta_e = 0.3\pi$ (Weak Kerr)									
6.....	0.351	−6.142	2.310	1.211	0.291	6.326	2.001	1.284	0.308
7.....	0.405	−5.916	2.680	1.164	0.271	6.122	2.301	1.246	0.285
8.....	0.459	−5.687	3.213	1.116	0.245	5.913	2.746	1.207	0.255
9.....	0.513	−5.447	3.971	1.066	0.217	5.691	3.394	1.164	0.222
10.....	0.567	−5.188	5.064	1.013	0.188	5.446	4.346	1.117	0.189
$P = 1.56$ ms; $\theta_e = \pi/2$ (Weak Kerr)									
6.....	0.434	−4.770	3.085	0.937	0.362	4.948	2.641	1.008	0.380
7.....	0.500	−4.519	3.922	0.885	0.318	4.715	3.351	0.964	0.328
8.....	0.567	−4.252	5.239	0.838	0.270	4.463	4.496	0.915	0.272
9.....	0.634	−3.596	7.377	0.771	0.222	4.177	6.400	0.859	0.218
10.....	0.701	−3.621	11.073	0.703	0.177	3.845	9.767	0.793	0.168
$P = 1.56$ ms; $\theta_e = \pi/2$ (Schwarzschild)									
6.....	...	−5.375	1.912	1.075	0.453	...	1.523	1.075	0.568
7.....	...	−5.312	2.120	1.063	0.418	...	1.630	1.063	0.543
8.....	...	−5.266	2.444	1.053	0.369	...	1.815	1.053	0.497
9.....	...	−5.231	2.949	1.046	0.310	...	2.115	1.046	0.432
10.....	...	−5.203	3.771	1.041	0.245	...	2.611	1.041	0.354
$P = 33$ ms; $\theta_e = \pi/2$ (Weak Kerr)									
6.....	0.020	−5.368	1.258	1.073	0.690	5.377	1.245	1.076	0.694
7.....	0.024	−5.304	1.218	1.060	0.730	5.315	1.203	1.064	0.735
8.....	0.027	−5.258	1.190	1.050	0.762	5.270	1.173	1.055	0.767
9.....	0.030	−5.221	1.169	1.043	0.785	5.234	1.151	1.048	0.792
10.....	0.033	−5.192	1.154	1.037	0.805	5.207	1.134	1.043	0.812

NOTE.—$Z^{\pm} = [1 + z(\pm 5°)]^3$; $\varphi_0(\delta = 0)$ has been subtracted from $\varphi_0(\pm 5°)$ values.

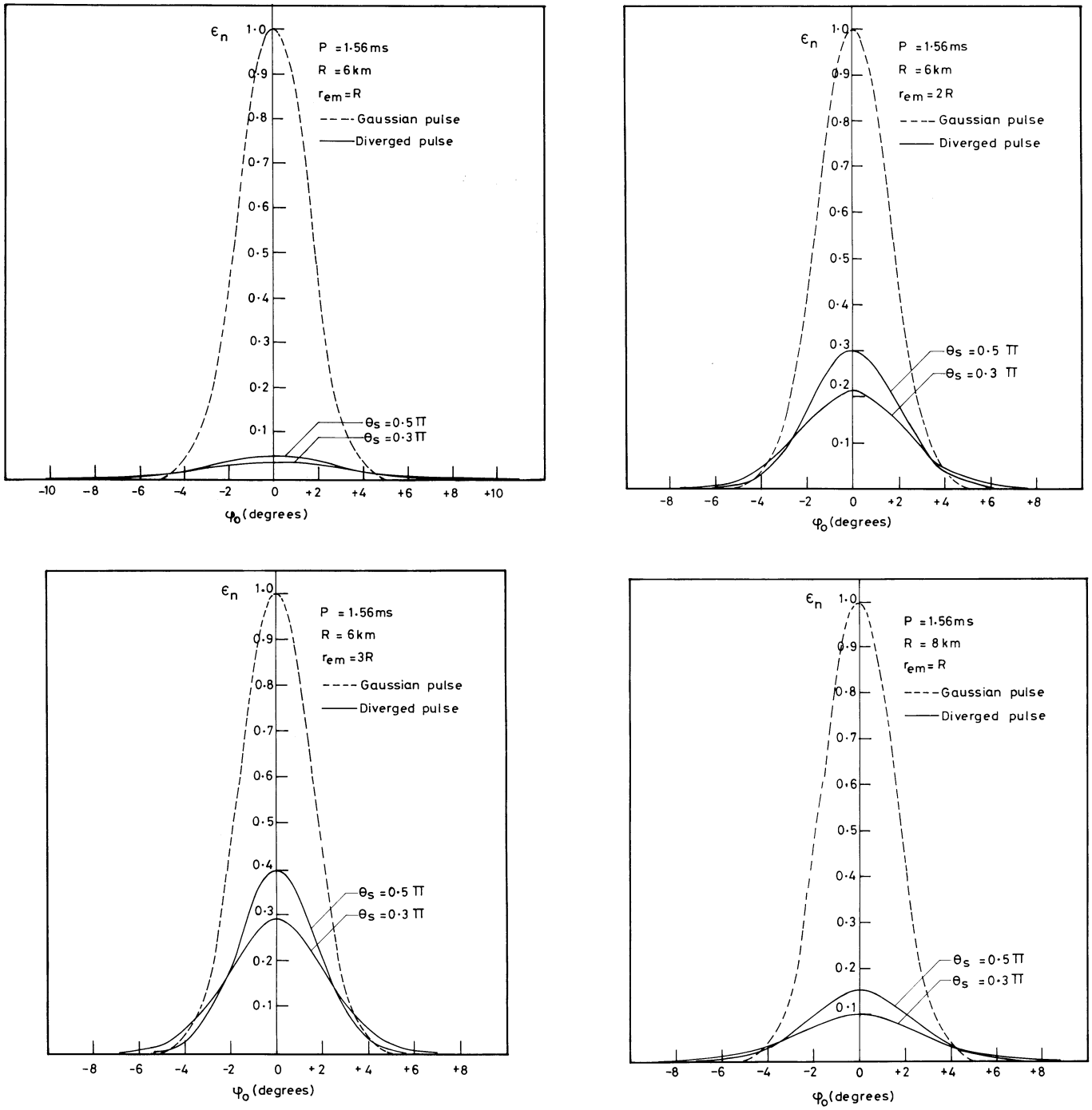

FIG. 2.—Net deamplification $\epsilon_n = I_n/I_e$ in the pulse as a function of longitude for two values of θ_e for the case $P = 1.56$ ms. The different figures correspond to the various neutron star radii and different radial locations r_{em} of the points of emission. The dashed curves are for an initial Gaussian profile and a beamwidth $W_e = 10°$ in the emitter's frame of reference.

beamwidth has a strong dependence on the tangential velocity of the emitter:

$$W_0 \simeq \frac{2 \sin \delta_e}{\sin \theta_e \, e^v} \frac{1 - V_e^2}{1 - V_e^2 \sin^2 \delta_e} \sim \frac{W_e}{\sin \theta_e} \left(\frac{1 - V_e^2}{e^v} \right) \text{(radians)}, \tag{22}$$

and consequently $W_0 < W_e$. For instance, when $r_{em} = 5\,R$, the $-5°$ photon is mapped at the longitude 3°.845, whereas the $+5°$ photon emerges at $-3°.621$, so that $W_{0(\text{Kerr})} = 7°.466$. In contrast, $W_{0(\text{Schw})} = 10°.406$. Thus a general consequence of aberration is that $W_{0(\text{Schw})} > W_{0(\text{Kerr})}$. For the shorter of the periods and emission in the equatorial plane, we find that the aberration effect on the beam dominates the divergence, making $\Delta^{\pm} < 1$ (and consequently $\epsilon^{\pm} > 1$) once $r_{em} \geq 25$ km (where $V_e \simeq 0.3$), regardless of the neutron star radius (Fig. 3). Although this would imply a slight increase in the pulse intensity over that of emission, as was pointed out by Bhatia et al.

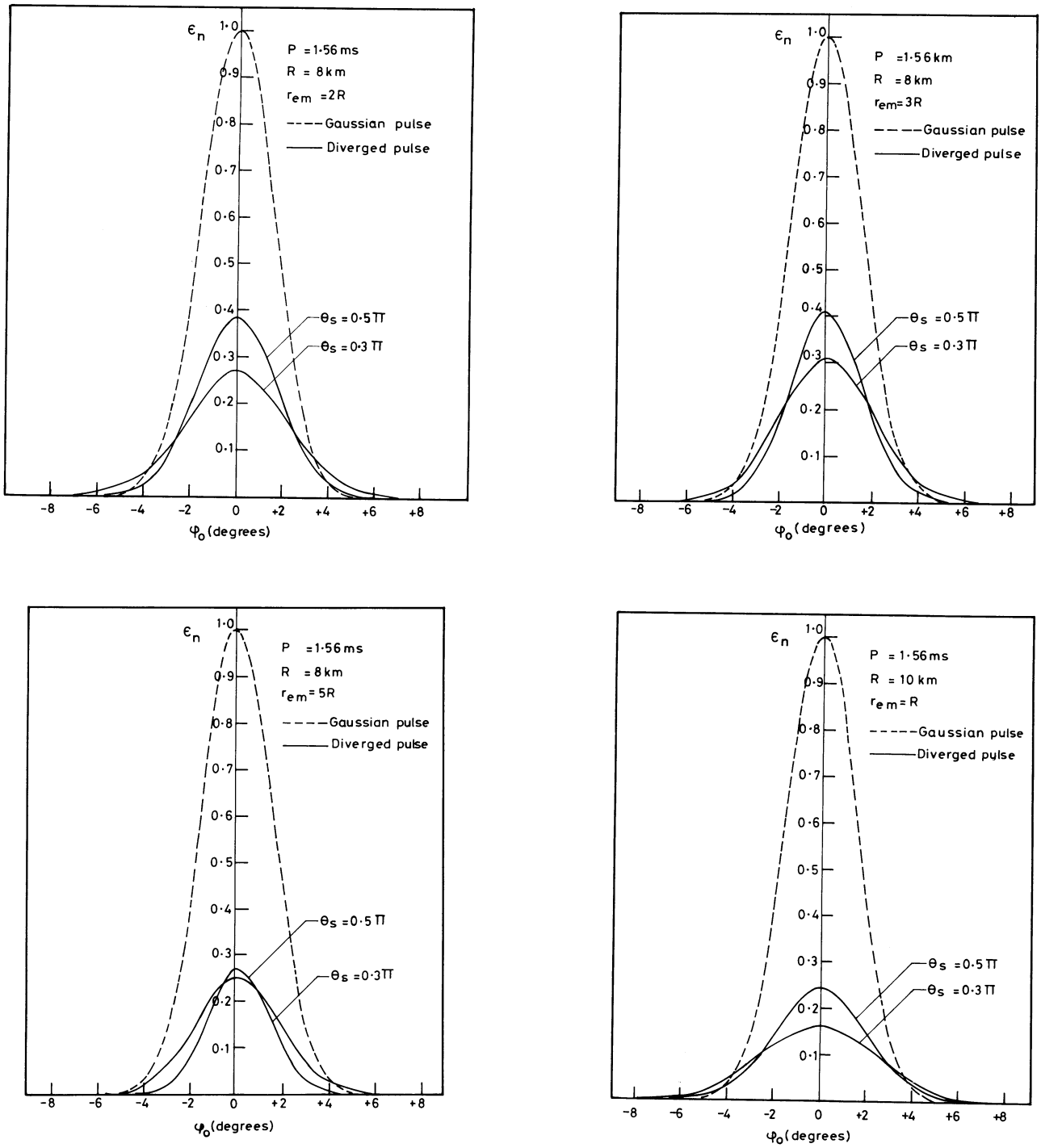

FIG. 2—*Continued*

(1988), the transverse Doppler redshift arrests any such increase to keep the resultant pulse profile flattened (Fig. 2). The squeezing effect is the strongest for emission in the equatorial plane. For the case of $\theta_e = 0.3\pi$, the squeezing has yet to catch up with divergence even at $r_{em} = 50$ km. On the other hand, for the slower rotation rate, we find $\Delta \leq 1$ when $r_{em} \geq 500$ km (at which point $V_e \simeq 0.3$).

Therefore, an earlier conclusion that the brightness temperature is larger in the emitter's frame than that inferred observationally by roughly an order of magnitude (Kapoor & Datta 1985) remains tenable for a millisecond pulsar whatever the location of the emission region in the context of the polar cap models. For slower pulsars, this is so only for $r_{em} < 20$ km. This is explicit in the plot for $I_n(\delta = 0)/I_e$ versus r_{em} (Fig. 4). In Figure 5 the x-axis has r_{em} in actual units, and all the curves corresponding to the various radii merge into one for the respective periods. For $P = 1.56$ ms, the curves turn over around $r_{em} \simeq 20$ km. It is in this region that the reduction in the

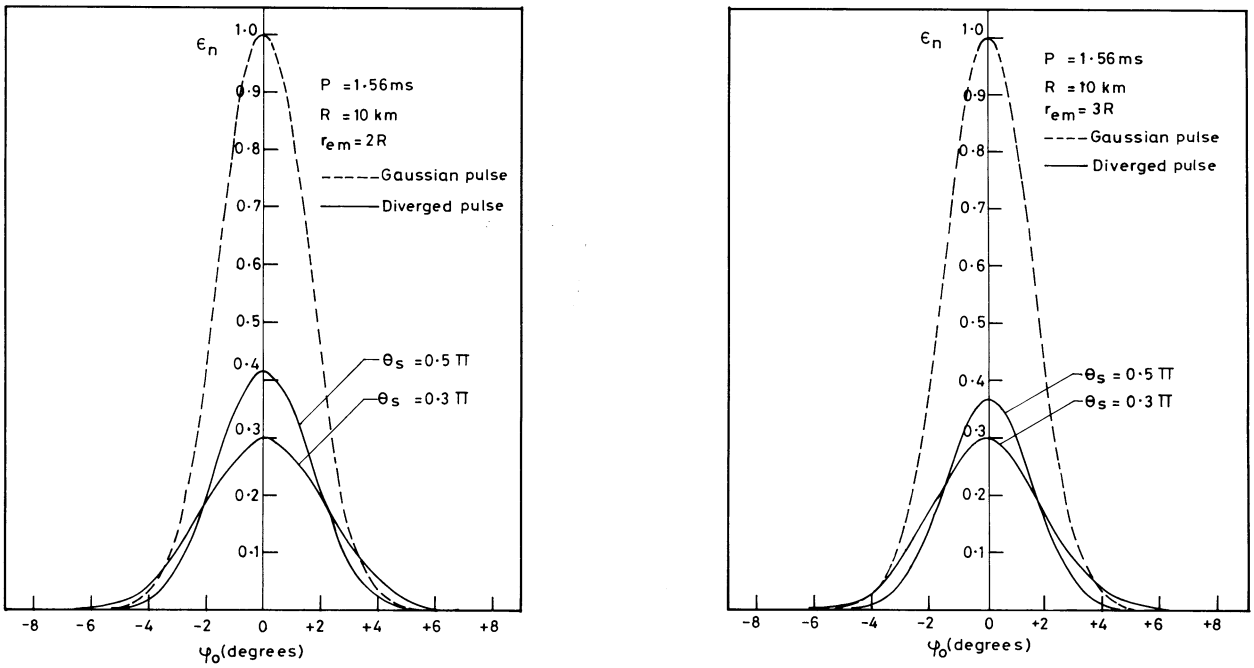

FIG. 2—*Continued*

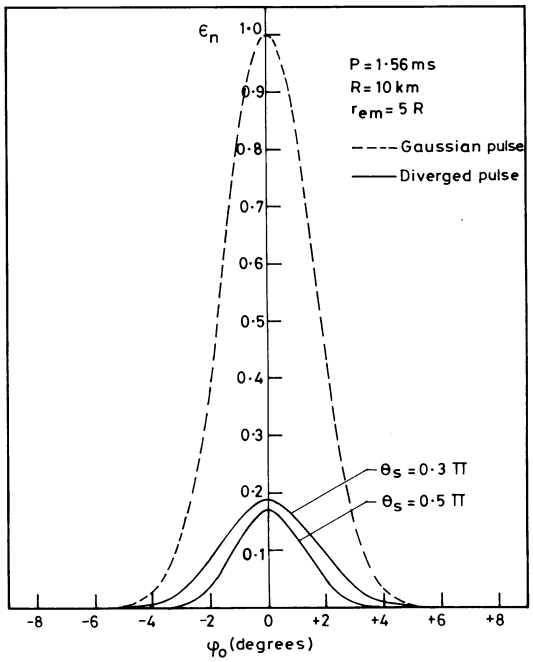

FIG. 2—*Continued*

intensity in the beam due to the relativistic effects will be least severe. In comparison with Figure 3 for W_0 versus r_{em}, the turnover in the $I_n(\delta = 0)/I_e$ curve occurs slightly earlier than that in the W_0 curve as r_{em} is increased.

From the multifrequency timing observations over the frequency range 0.3–1.4 GHz, Cordes & Stinebring (1984; see also Cordes et al. 1990) have suggested that the emission region for the millisecond pulsar 1937+214 is thin, being $\simeq$4 km. A calculation by Kapoor & Datta (1986) based on equations (19)–(21) then showed that arrival time differences far exceed the reported time-of-arrival discrepancy of 5–6 μs and concluded that the emission region must be thinner still. In Table 6 we list the results of calculations from equations (19)–(21) of advancement in the arrival time of a beam emanating from $r_{em} + \Delta r$ over that emitted from r_{em} as due to differences in the tilt angle $\varphi_0(\delta = 0)$ at the two radii and light travel time across Δr for $\Delta r = 1$ km. Since neutron stars with smaller radii are considered here, the retardation effect on the light travel time, $\Delta\tau_{ret}$, is more pronounced in comparison with a $\Delta r/c$ calculation. The values of $\Delta\tau_{ret}$ have a feeble θ_e dependence and increase as θ_e is increased. They are largest for the smallest of the neutron stars considered. The $\Delta\tau_{ret}$ values decrease as r_{em} is

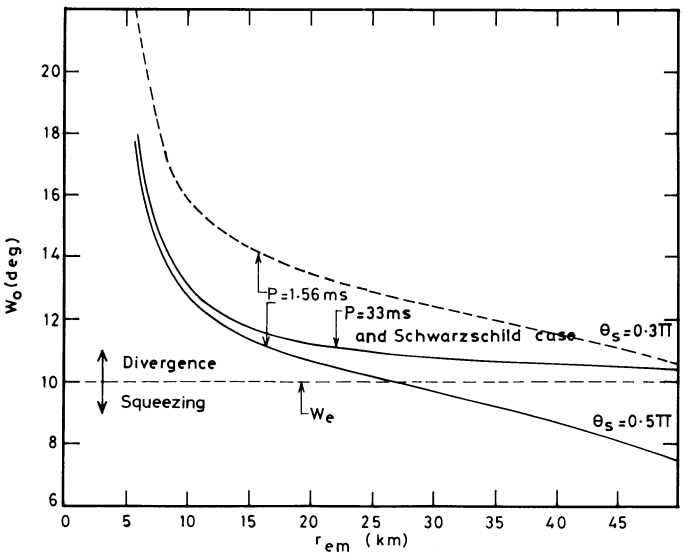

FIG. 3.—Variation of the width W_0 of the diverged beam (in degrees) as a function of radial location r_{em} of the points of emission.

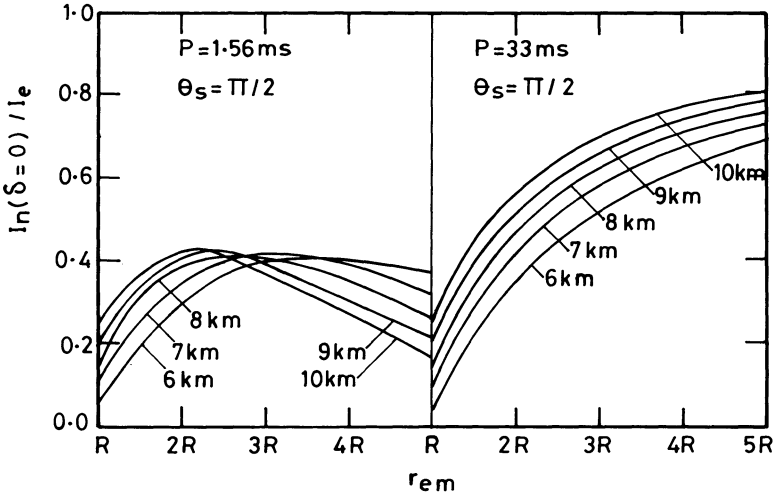

FIG. 4.—Net deamplification in the center of the diverged pulse as a function of radial location r_{em} of the points of emission in units of the neutron star radii considered.

increased, reaching a minimum near $3R$, and then increase again as a result of the influence of a larger V_e, except in the case of the 6 km configuration, where the Doppler contribution has yet to be pronounced. Also, the $\Delta\tau_{ret}$ values differ from the corresponding Schwarzschild values by tens of nanoseconds. The net arrival time advancement $\Delta\tau$, however, remains within $\simeq 8$–12 μs despite a large range in the values of R and r_{em} we have considered. To be consistent with the observations, the aberration and retardation effects thus constrain the thickness of the emission region to less than 1 km in the case of the millisecond pulsar 1937+214.

For an altitude of emission up to several neutron star radii this inference holds and would not be significantly altered if one were to include the effect of magnetic field line sweepback (Shitov 1983), which contributes negatively to the (lower frequency) pulse arrival time advancement introduced by aberration and retardation by an approximate amount

$$\Delta\tau_{ms} \sim \frac{3.6 \sin^2 \theta_e}{r_L^3} \frac{P}{2\pi} r_{em}^2 \Delta r \text{ s} , \qquad (23)$$

r_L being the light-cylinder radius. For the $P = 1.56$ ms case, $\Delta\tau_{ms}$ will be less than about 1 μs if emission takes place from $r_{em} \leq 20$ km. For a higher altitude, say $r_{em} = 30$ km, $\Delta\tau_{ms} \simeq$ 1–2 μs, indicating that with $\Delta r \simeq 1$ km one is close enough (see Table 6) to the observed time delay discrepancy. On the other hand, if $r_{em} = 50$ km, mutually compatible values of $\Delta\tau$ and $\Delta\tau_{ms}$ will result if the emission region is slightly thicker, i.e., $\Delta r \simeq 1.5$ km (equatorial emission).

For the sake of completeness, we list in Table 7 values of the tilt angle $\varphi_0(0)$ corresponding to the 33 ms period also, for various r_{em}. Here, for instance, near the surface an emission region of thickness $\simeq 10$ km will introduce, in the case of an $R = 10$ km neutron star, an arrival time difference between two pulses at frequencies ν_1 and ν_2 of about 40 μs due to aberration effect alone, the retardation correction being of similar magnitude. In comparison, contribution of the magnetic field line sweepback to the arrival times of pulses at the two frequencies will be small.

It is to be pointed out that there is a net difference in the arrival time of photons emitted at δ and $\delta + d\delta$: the backward-emitted photons take longer in comparison, as a consequence of the rotational effects. We evaluate a quantity termed time delay:

$$\Delta T_A = T_A(+\delta_e) - T_A(-\delta_e) \qquad (24)$$

from equation (11) for the $P = 1.56$ ms case and find that it is largest for the equatorial emission and shows a consistent increase with r_{em}. However, it turns out to be less than the pulse duration of the diverged beam for the range of r_{em} considered, so that there is effectively no pruning and a complete pulse will be detected (Kapoor & Datta 1985).

To conclude, it is now apparent that the relativistic effects contribute to the duty cycle and the pulsar beaming, but their magnitude cannot be specifically gauged unless one pinpoints where the (radio) emission is generated. If pulsar emission originates very near the surface (Rankin 1990; Phillips & Wolszczan 1990) and if this is generally true, the spacetime curvature will enhance the duty cycle by causing the beam to diverge

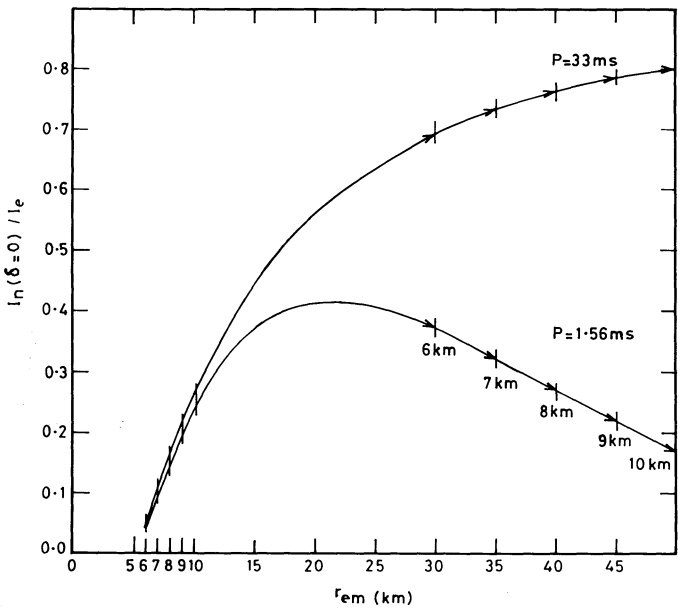

FIG. 5.—Same as Fig. 4, but for r_{em} in absolute units

TABLE 6

TILT $\varphi_0(r_{em}, \delta = 0)$, RETARDATION CORRECTION $\Delta\tau_{ret}$, AND NET ARRIVAL TIME ADVANCEMENT $\Delta\tau$[a]

R (km)	θ_e	$\varphi_0(r_{em})$	$\Delta\varphi_0$	$\Delta\tau_{drag}$ (μs)	$\Delta\tau_{ret}$ Schwarzschild (μs)	$\Delta\tau_{ret}$ Rotation (μs)	$\Delta\tau$ (μs)
				$r_{em} = R$			
6.....	54°	9°.419	0°.637	2.758	...	9.277	12.035
	90	9.408	0.645	2.790	9.249	9.294	12.085
7.....	54	8.921	1.032	4.466	...	7.487	11.953
	90	8.912	1.038	4.491	7.461	7.502	11.993
8.....	54	9.086	1.121	4.853	...	6.534	11.387
	90	9.079	1.127	4.876	6.506	6.550	11.426
9.....	54	9.504	1.134	4.908	...	5.942	10.850
	90	9.497	1.140	4.932	5.912	5.960	10.891
10.....	54	10.045	1.123	4.863	...	5.540	10.403
	90	10.039	1.130	4.888	5.505	5.559	10.447
				$r_{em} = 2R$			
6.....	54°	13°.450	0°.717	3.101	...	5.043	8.144
	90	13.475	0.723	3.131	4.985	5.074	8.205
7.....	54	14.712	0.760	3.288	...	4.736	8.025
	90	14.748	0.769	3.326	4.667	4.774	8.100
8.....	54	16.080	0.783	3.389	...	4.535	7.924
	90	16.130	0.794	3.435	4.451	4.581	8.016
9.....	54	17.511	0.797	3.451	...	4.396	7.847
	90	17.579	0.811	3.507	4.296	4.451	7.959
10.....	54	18.984	0.808	3.494	...	4.297	7.792
	90	19.075	0.823	3.563	4.178	4.364	7.927
				$r_{em} = 3R$			
6.....	54°	17°.867	0°.759	3.282	...	4.399	7.681
	90	17.947	0.771	3.338	4.296	4.457	7.795
7.....	54	20.083	0.780	3.374	...	4.262	7.637
	90	20.203	0.797	3.449	4.130	4.337	7.786
8.....	54	22.368	0.796	3.443	....	4.179	7.622
	90	22.540	0.818	3.539	4.013	4.275	7.815
9.....	54	24.705	0.809	3.503	...	4.131	7.634
	90	24.946	0.838	3.626	3.926	4.253	7.879
10.....	54	27.089	0.823	3.560	...	4.109	7.669
	90	27.418	0.859	3.715	3.859	4.262	7.977
				$r_{em} = 5R$			
6.....	54°	27°.271	0°.812	3.514	...	4.112	7.626
	90	27.616	0.848	3.670	3.859	4.267	7.937
7.....	54	31.350	0.837	3.623	...	4.118	7.741
	90	31.902	0.889	3.849	3.775	4.341	8.190
8.....	54	35.562	0.865	3.745	...	4.168	7.913
	90	36.414	0.941	4.070	3.714	4.485	8.555
9.....	54	39.928	0.899	3.889	...	4.258	8.148
	90	41.211	1.007	4.358	3.669	4.710	9.068
10.....	54	44.475	0.940	4.066	...	4.391	8.457
	90	46.384	1.098	4.752	3.633	5.046	9.798

NOTE.—$\Delta\varphi_0 = \varphi_0(r_{em} + \Delta r, \delta = 0) - \varphi_0(r_{em}, \delta = 0)$.

[a] For emission region thickness $\Delta r = 1$ km for the 1.56 ms period.

in longitude and latitude, and hence increase the beaming factor of the pulsars, even though only marginally. The smaller the radius of the neutron star, the greater the effect. If $r_{em} \geq 20$ km, the effects are minimal. This will hold for the millisecond pulsar too, where emission most likely emanates from near the surface and virtually the same altitude. On the other hand if r_{em} exceeds ≈ 30 km, the squeezing effect of aberration can overcome the divergence of the beam in longitude and thus reduces the duty cycle, particularly when the emission is in the equatorial plane. However, the latitudinal beamwidth remains virtually unaffected. Thus, for millisecond pulsars at least, the beaming factor cannot be correctly derived from a knowledge of the duty cycle alone. It is important to note that the divergence and the squeezing we have discussed above are over and above any other physical effect that may constrain the beamwidths as a function of r_{em} or the pulsar parameters. Calculations performed in a Schwarzschild background do not bring out many of these features, which fact alone underlines the importance of rotation in a general relativistic study of radiation characteristics of pulsars.

Here mention may be made of the studies by Pechenick, Ftaclas, & Cohen (1983) of the flattening of light curves from

TABLE 7

TILT ANGLE $\varphi_0(\delta = 0, r_{em}, \theta_s)$ ($P = 33$ ms; $M = 1.4\ M_\odot$)

R (km)	$\varphi_0(\delta = 0, r_{em})$	R (km)	$\varphi_0(\delta = 0, r_{em})$
$r_{em} = R$		$r_{em} = 3R$	
6.....	0.446	6.....	0.837
7.....	0.442	7.....	0.938
8.....	0.430	8.....	1.041
9.....	0.450	9.....	1.146
10.....	0.475	10.....	1.252
$r_{em} = 2R$		$r_{em} = 5R$	
6.....	0.633	6.....	1.259
7.....	0.691	7.....	1.437
8.....	0.755	8.....	1.615
9.....	0.821	9.....	1.794
10.....	0.888	10.....	1.973

NOTE.—$\varphi_0(\delta = 0,\ r_{em},\ \theta_e = 54°) \cong \varphi_0(\delta = 0,\ r_{em},\ \theta_e = 90°)$; $\Delta\varphi_0 = \varphi_0(r_{em} + \Delta r,\ \delta = 0) - \varphi_0(r_{em},\ \delta = 0)$, $\Delta\tau_{drag} = (\Delta\varphi_0)P/360°$.

the antipodal hot spots on the neutron star surface as a result of the lensing action of the star. Further, a similar study in a Kerr background by Chen & Shaham (1989) has indicated that the light curves depend strongly on the rotation speed and the emission spectrum and could become quite sharp and very nonsymmetrical as a consequence of large rotation, as opposed to the flattening effect of gravity. In their treatment all emission emanates from near the surface and virtually the same altitude. In contrast, our formalism, while referring to a narrow conical beam of monochromatic radiation, is frequency-independent but enables one to draw certain conclusions in the context of the radius-to-frequency mapping, a common feature of the polar cap models of the pulsar emission mechanism. We also find that, for the range of the radial location of the emission points considered here, light-curve asymmetries are quite small in extent. The pulse profile is affected in longitude more by aberration than by the Doppler boosting or diminution.

The author thanks Jagdev Singh and Prabhjot Singh for their help in computations.

REFERENCES

Bhatia, V. B., Chopra, N., Majumdar, B., & Panchapakesan, N. 1988, ApJ, 326, 63
Chandrasekhar, S. 1983, The Mathematical Theory of Black Holes (Oxford: Clarendon)
Chen, K., & Shaham, J. 1989, ApJ, 339, 279
Cordes, J. M., & Stinebring, D. R. 1984, ApJ, 277, L53
Cordes, J. M., Wolszczan, A., Dewey, R. J., Blaskiewicz, M., & Stinebring, D. R. 1990, ApJ, 349, 245
Joss, P. C., & Rappaport, S. A. 1984, ARA&A, 22, 537
Kapoor, R. C. 1979, Ph.D. thesis, Agra Univ.
———. 1981, Bull. Astr. Soc. India, 9, 232
———. 1990, in IAU Colloquium 128, The Magnetospheric Structure and Emission Mechanisms of Radio Pulsars, in press
Kapoor, R. C., & Datta, B. 1984, MNRAS, 209, 895
———. 1985, ApJ, 297, 413
———. 1986, ApJ, 311, 680
Lindblom, L. 1984, ApJ, 278, 364
London, R., Taam, R., & Howard, M. 1985, ApJ, 287, L27
Mészáros, P., & Riffert, H. 1987, ApJ, 323, L127
———. 1988, ApJ, 327, 712
Pechenick, K. R., Ftaclas, C., & Cohen, J. M. 1983, ApJ, 274, 846
Phillips, J. A., & Wolszczan, A. 1990, in Low Frequency Astrophysics from Space, ed. N. E. Kassim & K. W. Weiler (Berlin: Springer-Verlag)
Radhakrishnan, V., & Cooke, D. J. 1969, Ap. Letters, 3, 325
Rankin, J. 1990, ApJ, 352, 247
Shitov, Yu. P. 1983, Soviet Astr. 27, 314